A Study on Integral Design of Salt Crystallizers

C.J. Asselbergs and E.J. de Jong

Delft University of Technology, Laboratory of Chemical Process Equipment, Leeghwaterstraat 44, Delft, The Netherlands

ABSTRACT

An extensive experimental investigation has been carried out to study salt crystallizer behavior and performance for both units with external and internal heat exchanger. The general objectives of the work were to gain a deeper understanding of the phenomena which play a role, so that salt crystallizer design becomes more of a science and less of an art.

Based on the results of the investigation, a design procedure for salt crystallizers is put forward. This procedure comprises calculation of pressure loss and heat transfer surface area, and also a correlation of mean crystal size as a function of operating conditions. The latter correlation is derived from nucleation and growth kinetics, which have been determined experimentally.

A computer program has been developed which can be used for optimization of design in cooperation with the NEM (Leiden, Holland), as manufacturer of salt crystallizers.

INTRODUCTION

Crystallization of sodium chloride is by necessity effected by evaporation because the solubility is scarcely a function of temperature. Most evaporating crystallizers used in modern industrial practice are of the forced circulation (mixed suspension), circulating magma type. These crystallizers typically produce salt with an average size in the range of 400–600 μm. Users specifications for white salt include purity, shape and size distribution (mean size and uniformity) of the crystals. The latter basic properties affect the flow, handling, storage and packaging characteristics of the crystalline material. Designers of industrial crystallizers are thus faced with the problem of predicting the crystal size distribution (CSD) with sufficient accuracy. The reliability of most design methods is, however, poor due to the shortage of pertinent data concerning crystallization kinetics and process configuration. The lack of data, applicable to industrial systems, arises from the complexity of the unit operation of crystallization. Crystallization is governed by complicated processes, that through their interaction generate the crystal size distribution. Some insight into the mechanisms of crystallization may be provided by the information flow diagram depicted in Figure 1: the product magma concentration is determined by the mass balances and the solubility curve. The degree of supersaturation is determined by the rate of evaporation, the rate of discharge as well as by the total crystal surface area in the vessel. The supersaturation then is the driving force for the rate of formation of nuclei and the rate of growth, which both are influenced by the suspension hydrodynamics. The nucleation rate is moreover dependent on the magma concentration. Nucleation and growth kinetics and the mean crystal residence time as a function of particle size, which depends on suspension hydrodynamics, finally determine the crystal size distribution through the numbers balance. The latter states that the number of particles within any given size range must be conserved at steady state. The crystal surface area available for deposition follows from the CSD, thus completing the feedback loop.

Although crystallization is known to be a very complex operation, rapid progress has been made in the past decade through quantitative techniques based on the numbers or population balance. The numbers balance is a powerful tool for the analysis and prediction of the performance of particulate systems, that has opened the possibility to extract the nucleation rate and the growth rate simultaneously from the crystal size distribution of a Mixed Suspension, Mixed Product Removal (MSMPR) system. This has led to both empirical correlation of crystallization kinetics and to fundamental nucleation mechanism studies. As a result a

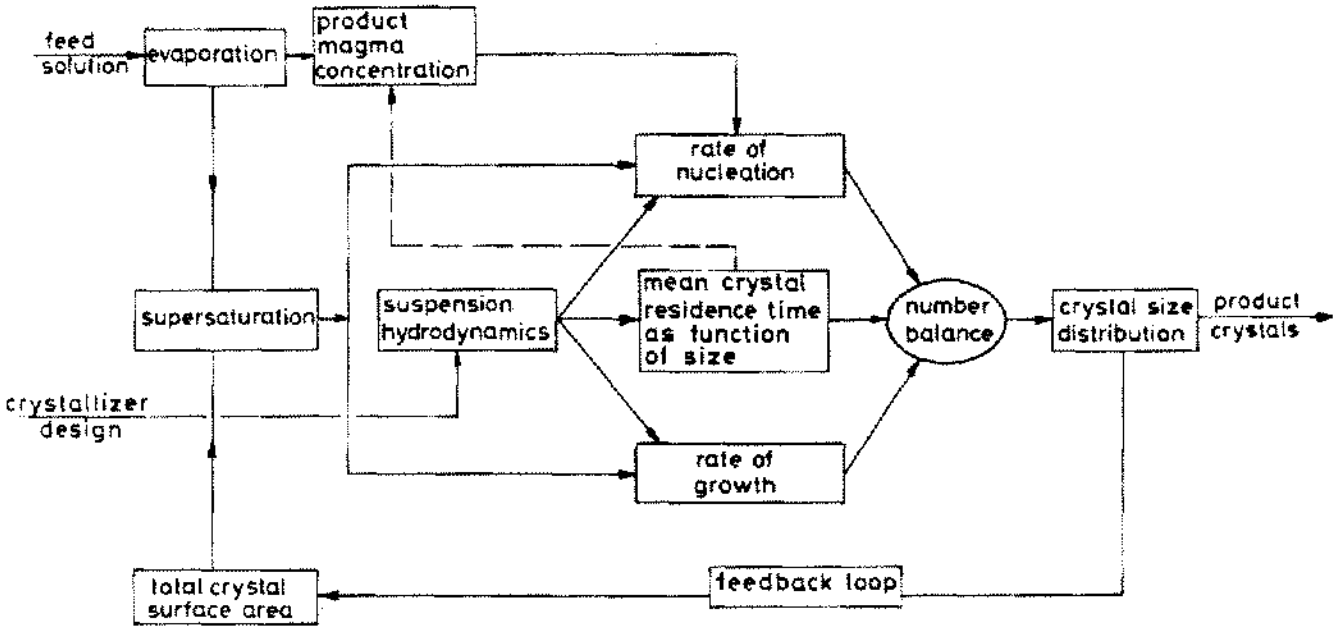

Figure 1. Crystallization information flow diagram.

number of crystallizer design procedures based on number balance techniques has been put forward. The key to success of these procedures lies in the availability of kinetic data and in adequate modeling of the actual commercial system in terms of the numbers balance. Although crystallization kinetics may be readily obtained from small-scale MSMPR units, application of the data to design of large-scale units may be rather hazardous, since the effect of scale on nucleation and growth is in general not fully understood. Consequently, if the design possibilities using the numbers balance are to be exploited to their full advantage, information must be available derived both from laboratory MSMPR equipment and from pilot scale crystallizers, wherein the production regime of crystallization is reproduced.

The present paper deals with the selection and design of evaporative salt crystallizers. The relative merits of the two basic types of evaporator (viz. internal and external circulation) will be discussed and a brief summary will be given of the results of a concomitant experimental and theoretical study in assessment of design criteria for salt crystallizers. Attention will be focused on the development of a blueprint for design of internal calandria systems comprising numbers, material and energy balance equations. Furthermore requirements of heat transmission and hydraulic transport will be taken into account.

An important feature of the design model will be the development of two relations for crystallization and heat transfer respectively, which describe the working volume of the crystallizer as a function of the pump impeller power input per unit mass of slurry. The present design procedure can be used for process optimization and is an extension of the model for design of stirred tank cooling crystallizers, presented in a previous paper (1). The method will be illustrated for the case of a low temperature MSMPR evaporator and a rough estimate of the equipment costs of two variants will be given.

SALT CRYSTALLIZERS

Depending on the location of the heat exchanger, through which the heat for evaporation is introduced, two basic types of forced circulation equipment can be distinguished. The two designs, namely the internally and the externally forced circulation types of NaCl crystallizer are schematically shown in Figure 2. The main equipment characteristics are summarized in Table 1. In both cases agitation and circulation are caused by recycling of the slurry with an axial-flow pump (having a large capacity and low head). The circulating magma is heated in a single-pass long-tube vertical heat exchanger, which is placed far enough below the liquor level to suppress boiling in the tubes and at the top tubeplate. Thus salting (encrustation) within the tubes and tube blockage, which would reduce the circulation rate, are prevented. Both evaporators shown in Figure 2 may be fitted with an elutriation leg for purposes of counter-washing with fresh feed brine, thickening and classification of the product salt.

The internal circulation crystallizer, as shown in Figure 2, evolved from the standard short-tube vertical Calandria evaporator, which had low tube velocity (poor heat transfer), low circulation rate and non-uniform velocity distribution through the tubes. These basic weaknesses have been surmounted in the present design, which also features

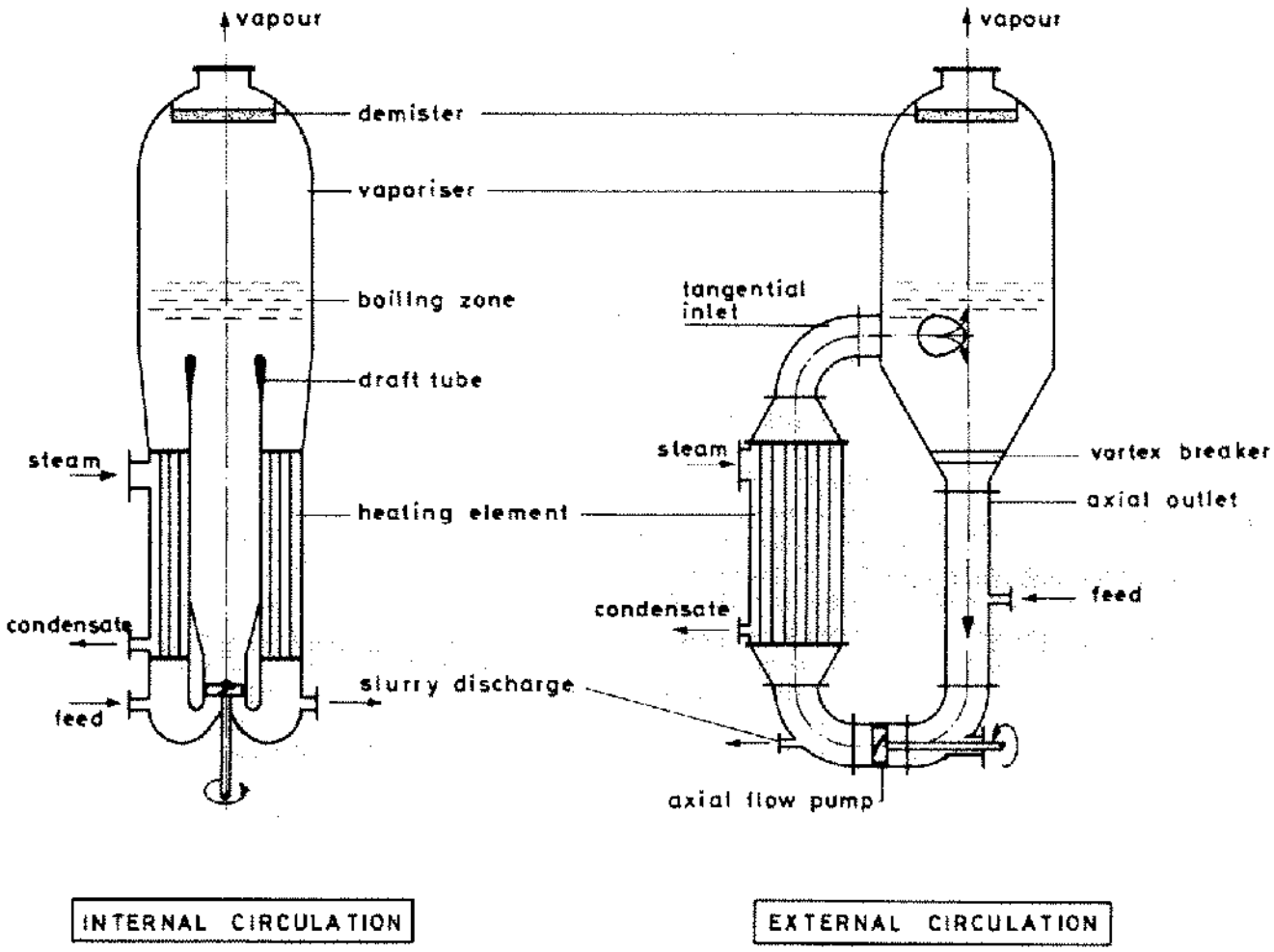

Figure 2. The two basic salt crystallizer designs.

a dished base designed to promote off-bottom suspension and eliminate stagnant zones underneath the draft tube. The magma may circulate either up the draft tube and down the annulus or vice versa. A serious drawback of internal calandria machines is the large-diameter annular tubeplate, which, especially for large-capacity units, may be an important cost-factor. Depending on operating conditions and plant capacity it may be necessary to provide the shell of an internal heater with bellows to prevent unacceptable thermal expansion stresses on the heater tubes.

For external circulation systems the design of vaporizer and heating element do not interdepend and the latter generally features a more convenient length to diameter ratio. Compared with the swirling flow pattern created by the submerged tangential inlet in external circulation crystallizers, the flow pattern in internal circulation systems is far less complicated. Since the main direction of flow in the latter is vertical (versus horizontal in the former case) the crystals may be more effectively carried up to the boiling zone where they grow. An additional advantage of the vertical flow pattern lies in the relative simplicity of scale-up. In the design of vaporizers with horizontal tangential inlet and vortex breaker (to eliminate excessive vortex-formation in the pump suction line) both the Froude number and the ratio between vaporizer diameter and inlet diameter play a prominent role. Due to the presence of circulation piping and bends, external circulation is achieved against higher heads and, therefore, requires more power per ton capacity than an internal circulating loop.

An important factor in the design of evaporators is the boiling behavior. Reliable data concerning the maximum allowable vapor velocity (which determines the vaporizer diameter) are normally wrapped in mystery and it has not been published whether internal circulation causes more uniformly distributed boiling than external circulation. In industrial practice vapor heads are frequently provided with mesh-type separators to minimize entrainment losses.

The liquor level in external circulation machines must be kept appreciably above the tangential inlet in order to suppress boiling and prevent salting within the inlet pipe. This

TABLE 1

Main Characteristics of Salt Crystallizers with Internal and External Circulation

	INTERNAL CIRCULATION	EXTERNAL CIRCULATION
Direction of main flow	axial	tangential
Heating element	expensive large-diameter annular tubeplate	heater and vaporizer design do not interdepend
Scale-up	simplicity of scale-up	similarity difficult to ensure (Froude)
Head requirements (power/ton capacity)	low	high
Construction	monolithic & compact	supporting steel work
Axial-flow pump	vertical	horizontal

method of operation, however, results in short-circuiting from inlet to bottom outlet of liquor that has not flashed to equilibrium at the pressure in the vaporizer (2). Short-circuiting results in an increase of the temperature level of the liquor circulating through the heat exchanger, hence in an undesirable decrease of the logarithmic mean temperature difference available for heat transfer between the heating steam and the circulating magma. Although comparative studies of short-circuiting have not been reported, it may be expected that the degree of short-circuiting will be less in internal circulation machines.

Few studies are available on the effects of operating conditions and crystallizer design on mean crystal size and crystal size distribution in manufacturing plants. On the basis of the work of van 't Land et al. (3, 4) it may be inferred that internal circulation systems are capable of producing coarser salt than crystallizers with external circulation and that crystallizer design affects median crystal size more distinctly than operating conditions. The CSD in terms of population density of white salt was moreover found to deviate from the straight line which the numbers balance thoery predicts for MSMPR systems. This deviation seemed less for internal calandria units. It should be noted however that the observations of the above workers may be particular to the systems studied and thus lack general validity.

From the foregoing considerations it may be evident that both types of salt crystallizers have their merits and that the present state of knowledge does not permit an unequivocal choice between the two alternatives.

SUMMARY OF EXPERIMENTAL WORK

An engineering-oriented study has been carried out during the past years to gain a deeper understanding of crystallization behavior, particle mechanics (segregation and classification) and scaling-up of salt crystallizers. Continuous crystallization experiments have been performed both in a 50 liter evaporative MSMPR crystallizer and in a 10 t/day capacity model of an industrial evaporator with tangential inlet and bottom central outlet (external circulation). The latter semitechnical unit was designed so that the industrial crystallization environment was appropriately reproduced. The MSMPR crystallizer featured a hollow draft tube fitted with a low-clearance impeller and a special dished base to improve crystal suspension. Full details of the experimental and theoretical work are given elsewhere (5). Some important observations and conclusions are summarized below.

The population density distributions of the salt produced in the pilot-scale evaporator with tangential inlet were similar to those found industrially (deviating from the ideal MSMPR distribution). Mixing of the solid phase was found

to be very poor: uniform suspension of the crystals was not attained and considerable radial maldistribution of solids occurred. The results of the work indicated that this phenomenon of internal classification influenced the CSD both directly, through residence time distribution, and indirectly, through selectively exposing the growing crystals to spatial variations of supersaturation. Thus, it was inferred that classification contributes significantly to the anomalous shape of the population density distribution generally found for industrial NaCl crystallizers with external circulation.

Since it was demonstrated that the degree of classification could not be appreciably reduced by changing operating conditions, an additional series of experiments was performed with reversed external circulation. By axial introduction of the magma, crystals were carried up more effectively to the boiling zone and the larger particles were retained in the evaporator body rather than circulated through the circulating line. This may lead to suppression of both primary and secondary nucleation. Median crystal sizes were generally found to be larger for the case of reversed circulation than for tangential flow operation. It was moreover demonstrated that thermal short-circuiting was virtually non-existent and that boiling was uniformly distributed and definitely not more vigorous than in conventional operation. The experiments thus strongly suggested that the unfavorable effects of classification and short-circuiting in tangential inlet machines can be offset by reversing the direction of external circulation.

The 50 liter crystallizer with draft tube agitation was shown to conform to the MSMPR concept. The crystal growth rate of NaCl was independent of crystal size except when rounded particles were produced due to abrasion. Nucleation and crystal growth rates were obtained from experimental crystal size distributions and could be described over a wide range of operating conditions by power law kinetics of the form

$$\frac{B^0}{M_{si}} = 1.9 \times 10^{19}\, \epsilon^{2/3}\, G^2 \quad (\#/s.\ kg\ crystals) \qquad (1)$$

where B^0 is the rate of nucleation, M_{si} is the magma concentration, ϵ is the impeller power consumption per unit mass of slurry and G is the linear crystal growth rate. Relation (1) applied to both a propeller and a pitch blade type of agitator. The power consumption, ϵ, contains the impeller power number representing the effect of impeller design. The mode of nucleation was predominantly secondary and the rate of nucleation at constant impeller speed was lowest when the propeller was used.

SALT CRYSTALLIZER DESIGN PROCEDURE

Choice of crystallizer. External circulation crystallizers are successfully operated in industry and their design is in most cases based on extensive past experience on scales not too far removed from the evaporator to be designed. However, when product specifications are very strict, design of these machines tends to be difficult because information regarding classification and distribution of supersaturation in large-scale evaporators is not available. The concept of reversed external circulation proposed earlier, offers distinct advantages over the tangential flow system, but still lacks the maturity to justify application on the large-scale. The simple vertical flow pattern in units with internal circulation is capable of producing a well-mixed crystal suspension with uniform properties. These systems may therefore effectively approach a MSMPR crystallizer and the above kinetics of crystallization, though derived on a much smaller scale, can be used by first approximation in the numbers balance based design of internal calandria crystallizers. For MSMPR crystallizers a coefficient of variation of 50% is predicted which is relatively high and may be undesirable commercially. This may be obviated by employing an elutriation leg for purposes of classification at the cost of MSMPR behavior. The definite choice of crystallizer will depend on economical considerations (e.g. comparison of over-all plant cost) which are not easy to judge from an academic point of view.

The integral design procedure proposed in the present paper will be illustrated for an internal calandria evaporator. The geometry and basic design parameters of the unit chosen are depicted in Figure 3. The direction of flow is down the draft tube. The base of the crystallizer is formed so that magma velocities are sufficiently high and off-bottom suspension is attained. The draft tube extends beyond the heating element on both sides, to promote uniform flow distribution through the heater tubes and suppress short-circuiting. An important design parameter affecting the hydrodynamics in the vaporizer is the ratio of draft tube velocity and annular velocity, β. A second parameter, α, is defined as the ratio between the heater tube inner diameter, D_t, and the pitch of the tubes, p, and determines the heater tube velocity for given value of the velocity in the annulus. The vaporizer shell may in practice be fitted with a conical section between boiling zone and heater, to reduce the diameter of the heater tube plates. For reasons of simplicity the present design method is limited to cylindrical vessels of constant diameter. The walls of the crystallizer and the tubeplates are made in monel-clad and the heater tubes in cupro-nickel.

The following aspects of the design of the internal circulation system shown in Figure 3, will be discussed in the next sections. These are material, energy and population balances, entrainment, crystallization kinetics, heat transfer, internal loop pressure drop, and suspension of crystals. Equations will be developed which will be subsequently used to calculate the main equipment dimensions for a given set of design input variables (e.g. rate of production, median crystal size, heater tube diameter).

Material balances. In formulating the material balances

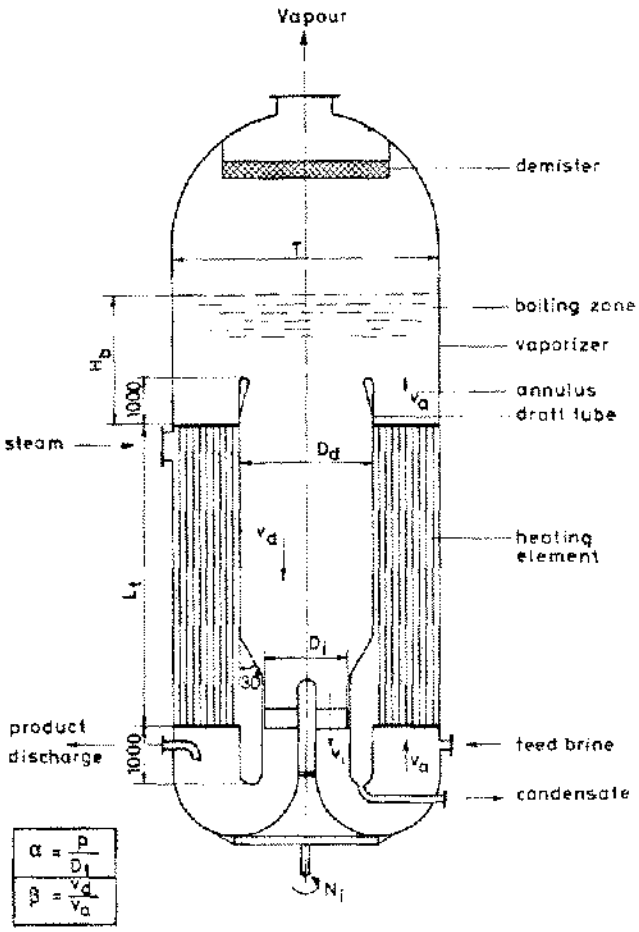

Figure 3. Internal calandria crystallizer design.

over a crystallization system the choice of the various process parameters and their dimensions is rather important. For the present development the definition of the symbols is given in Figure 4. For a binary system with one feed stream containing no crystals, one product stream and evaporation of the solvent (parallel feed, parallel product discharge) the general balance equations are

overall mass balance:

$$\phi_{mf} = \phi_{mps} + \phi_{mpl} + \phi_{mv} \quad (kg/s) \tag{2}$$

solute balance:

$$\phi_{vf} c_f = \phi_{vpSL} M_{SL} + \phi_{vp\cdot L} c_p \quad (kgNaCl/s) \tag{3}$$

The magma concentration, M_{SL}, is based on unit suspension volume and in the overall mass balance a distinction is made between a crystal mass flow rate, ϕ_{mps}, and a mother liquor mass flow rate, ϕ_{mpl}. Thus the contribution of the solid phase to the volumetric and mass flow rate has not been neglected in this case. The balance equations can be solved to give a relation for the magma concentration which reduces to

$$M_{SL} = \frac{\phi_{mv}}{\phi_{vpSL}} \cdot \frac{c_f}{\rho_{Lf} - c_f} \quad (kg/m^3) \tag{4}$$

when composition and liquor density of feed and product stream are approximately equal, or more rigorously

$$\frac{\rho_{Lp}}{\rho_{Lf}} = \frac{c_p}{c_f} \tag{5}$$

Since the rate of salt production, P, is given by

$$P = \phi_{vp\,SL} M_{SL}, \tag{6}$$

equation (4) can be directly used to evaluate the rate of evaporation, when P and the feed conditions are given

$$\phi_{mv} = \frac{\rho_{Lf} - c_f}{c_f} \cdot P \quad (kg/s) \tag{7}$$

The magma concentration is fixed when in addition to the rate of product withdrawal has been chosen (or vice versa).

The vaporizer diameter, T, can be calculated from the vapor load using entrainment correlations. The maximum allowable vapor velocity is normally given in terms of vapor velocity head or the square root of the relative vapor-liquid density difference. The vapor load per unit cross-sectional area of vaporizer may thus be readily evaluated for a given vapor temperature.

Energy balance. The total heat flow, ϕ_w, which has to be transferred to the system is described by the energy balance

$$\phi_w = \phi_{mf} C_{pf} (T_f - T_p) + Q_{cr} P + \phi_{mv} r \tag{8}$$

where C_{pf} is the specific heat of the feed brine, Q_{cr} is the heat of crystallization and r is the heat of vaporization. The heat of crystallization is very small for salt and may be neglected. The heat flow necessary for evaporation of the solvent is much larger than the first term on the right-hand side of Eq. (8).

Population balance. The complete modeling of an industrial crystallizer in terms of population balance equations is at present only possible for relatively simple systems. For Mixed Suspension Mixed Product Removal (MSMPR) crystallizers, which are substantially well-mixed, without internal classification or classification at the product off-take point, and where the effect of breakage and attrition may be neglected, the steady state population balance may be written (6)

$$\frac{\delta(Gn)}{\delta L} = -\frac{n}{\tau} \tag{9}$$

where G is the linear crystal growth rate, n is the population density of crystals of size L and τ is the draw-down time.

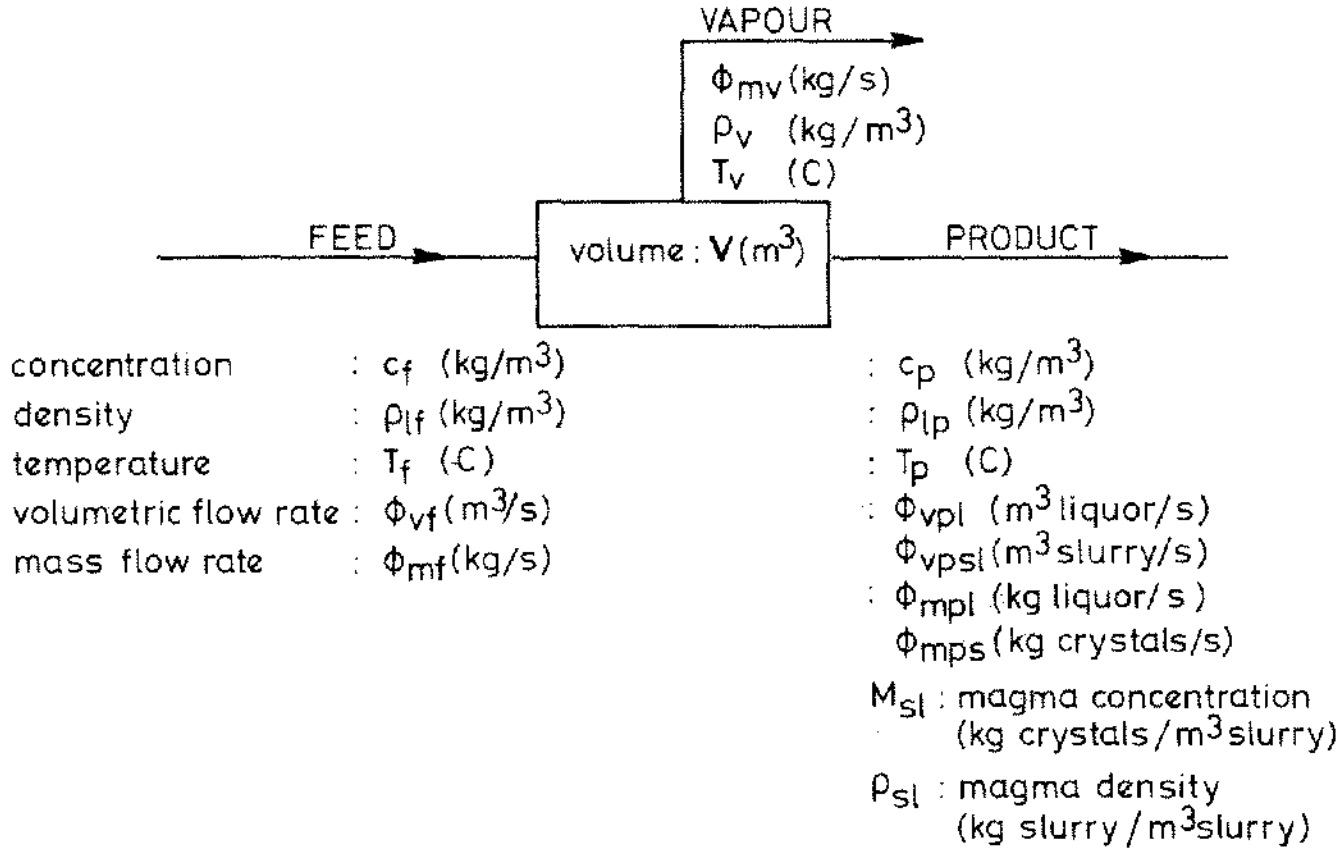

Figure 4. Definition of variables.

When the growth rate is independent of size, this equation can be solved to give

$$n = \frac{B^o}{G} \exp\left(-\frac{L}{G\tau}\right) \qquad (\#/m.m^3 \text{ slurry}) \qquad (10)$$

where B^o is the rate of nucleation. This relation uniquely determines the crystal size distribution in terms of crystallization kinetics and draw-down time. The magma concentration, M_{SL}, can be obtained from the third moment of the above crystal size distribution

$$M_{SL} = 6k_v \rho_s \frac{B^o}{G} (G\tau)^4 \qquad (kg/m^3) \qquad (11)$$

where k_v is a volume shape factor and ρs is the density of the crystals. For MSMPR conditions it can be shown (6) that the median crystal size of the product (50%, weight basis) is given by

$$L_{50} = 3.67\ G\tau \qquad (12)$$

The application of the above equations to design of industrial crystallizers may be hazardous, since many industrial systems do not obey the MSMPR concept. The basic population balance may be modified to take deviations of size dependent growth or classification into account, yielding equations similar to Eqs. (11) and (12) containing a parameter which may be a function of operating conditions (1). It has been alluded to previously that salt crystallizers with internal circulation may effectively approach a MSMPR system, especially when vertical velocities are sufficiently high to carry up crystals to the boiling zone and the axial-flow pump is designed so that crystal damage is minimized. The present design procedure will be based on the MSMPR concept.

Crystallization kinetics. In addition to the description of the crystal size distribution, suitable kinetic expressions are needed for crystallizer design. Since growth and nucleation rates cannot be calculated from first principles, the kinetics of crystallization must be determined experimentally. This may be readily achieved for laboratory scale MSMPR equipment. Nucleation and growth rates obtained in this way may be correlated by a power law expression of the form

$$B^o = k_n \epsilon^h G^i M_{SL}^j \qquad (\#/m^3 \text{ slurry.s}) \qquad (13)$$

where ϵ is the power input per unit mass of magma and k_n, h, i and j are empirical constants. The rate constant k_n is likely to depend on the presence of impurities, the temperature and the geometry of the system. It is assumed here that

nucleation is predominantly secondary in nature, hence the dependence on the specific power input (7). When equations of the above type are applied in commercial situations, it should be borne in mind that k_n and also h, i and j may be a function of the scale of operation.

Crystallization design relation. On the basis of the kinetic correlation, Eq. (13), and the expressions for the magma concentration, Eq. (11), and the median crystal size, Eq. (12), an equation can be derived which can be directly applied to crystallizer design. Elimination of B° between the first two equations and rearranging gives

$$(G\tau)^{i+3} = \frac{1}{6k_v\rho_s k_n} \cdot \epsilon^{-h}\, M_{SL}^{j-1}\, \tau^{j-1} \qquad (14)$$

By combination with Eq. (12), the median crystal size becomes

$$L_{50} = 3.67 \left\{ \frac{\epsilon^{-h} M_{SL}^{j-1}\, \tau^{j-1}}{6k_v\rho_s k_n} \right\}^{\frac{1}{i+3}} \qquad (15)$$

The median size characterizes the product and is an important input variable for crystallizer design. From Eq. (15) some important conclusions may be drawn: for example when $j = 1$, the magma concentration has no effect on the median particle size. The exponent i describes the relative kinetic order of nucleation and growth. When $i > 1$ the median size can be increased by increasing the mean retention time of the crystals.

Equation (15) can be rewritten in terms of the rate of production, P, and the crystallizer volume, V, since

$$\tau = \frac{V}{\Phi_{vp,SL}} = \frac{V\, M_{SL}}{P} \qquad (16)$$

Thus

$$L_{50} = k_c \left\{ \frac{M_{SL}^{j-1}\, V^{j-1}}{\epsilon^h\, P^{j-1}} \right\}^{\frac{1}{i+3}} \qquad (17)$$

where

$$k_c = 3.67\, (6k_v\rho_s k_n)^{-1/(i+3)} \qquad (18)$$

When the kinetic constants are known and the rate of production and the median size are given, Eq. (17) describes the relationship between V, M and ϵ. The correlation reduces to a function of two choice variables once the magma concentration is fixed. The crystallizer working volume is largely dependent on the brine level and the heater tube length as the vaporizer diameter is determined by the allowable vapor load. From heat transfer considerations it follows that, for a given heat load, the heater tube length (or heat-transfer surface area) depends upon the tube velocity and hence on the specific power input, ϵ. Thus a second correlation between ϵ and V may be derived on the basis of classical heat-exchanger optimization. This will be detailed below.

The power required for mixing and circulation will in a later stage also be represented by the power consumption per ton capacity of salt, ϵ', which may be calculated from the specific power input.

Heat-transfer. Neglecting the contributions of the feed and product stream, which are very much smaller than the rate of internal circulation, the energy balance becomes

$$\phi_w = \phi_{mv}\, r \qquad (19)$$

The total heat flow is determined by the rate of production and the feed composition via Eq. (7) and is equal to the heat flow to be transferred in the internal heater

$$\phi_w = U.A.LMTD \qquad (20)$$

where U is the over-all heat-transfer coefficient, A is the heat-transfer surface area and LMTD is the logarithmic mean temperature difference. The total heat load is also given by

$$\phi_w = \phi_{mc} c_{p,SL} \Delta T_c \qquad (21)$$

where ϕ_{mc} is the mass flow rate of circulation, $c_{p,SL}$ is the specific heat of the slurry and ΔT_c ($= T_o - T_i$) is the temperature rise through the heater. The rate of circulation can be written

$$\phi_{mc} = v_t \rho_{SL} N_t \frac{\pi}{4} D_t^2 \qquad (22)$$

where v_t is the tube velocity, N_t is the number of tubes, and D_t is tube inner diameter. The number of tubes may be approximated analytically via the parameters α and β

$$\alpha = \frac{P}{D_t} \qquad (23)$$

$$\beta = \frac{v_d}{v_a} \qquad (24)$$

or

$$\beta = \left(\frac{T}{D_a} \right)^2 - 1 \qquad (25)$$

For an equidistant triangular pitch of the heater tubes, it can be shown that the two-dimensional "porosity" of the tubeplate is

$$\text{porosity} = \frac{2\sqrt{3}\,\alpha^2}{\pi} \qquad \left(\frac{\text{m}^2 \text{ tube}}{\text{m}^2 \text{ tubeplate}} \right) \qquad (26)$$

Also

$$\text{porosity} = \frac{N_t \frac{\pi}{4} D_t^2}{\frac{\pi}{4}(T^2 - D_o^2)} \tag{27}$$

Combination of Eqs. (25), (26) and (27) gives

$$N_t = \frac{\beta}{1+\beta} \cdot \frac{\pi}{2\sqrt{3}} \cdot \left(\frac{T}{\alpha D_t}\right)^2 \tag{28}$$

The parameter α will be used later along with the heater tube outer diameter/pitch ratio.

The heat-transfer surface area based on tube outer diameter is

$$A = N_t L_t \pi D_{to} \tag{29}$$

where L_t is the tube length and D_{to} is the tube O.D.

Eqs. (19), (21), (22) and (28) yield

$$\Delta T_c = \frac{8\sqrt{3}}{\pi^2} \cdot \frac{r}{\rho_{SL} c_{pSL}} \cdot \frac{1+\beta}{\beta} \cdot \frac{\alpha^2}{T^2} \cdot \frac{\phi_{mv}}{v_t} \tag{30}$$

This equation can be used to evaluate ΔT_c as a function of α, β and v_t when the rate of production, the feed conditions and the crystallization temperature are known.

Referring to Figure 5 the logarithmic mean temperature difference can be written

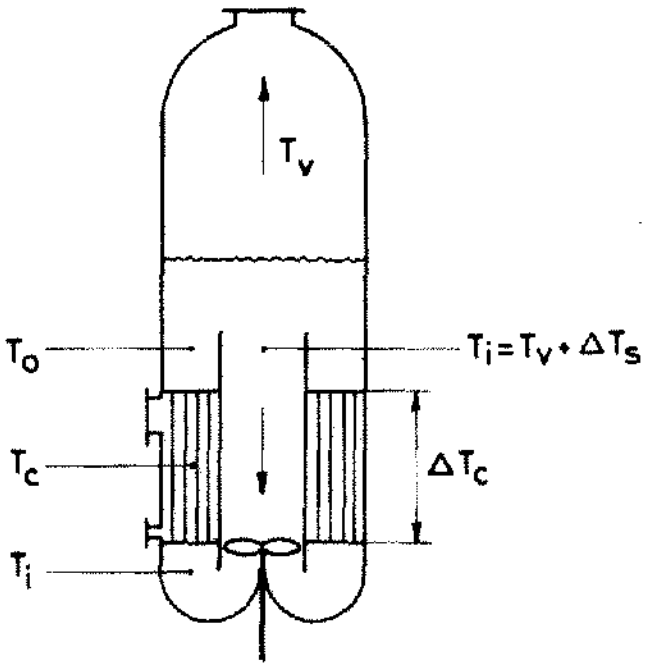

Figure 5. Definition of temperatures.

$$\text{LMTD} = \frac{T_v - T_i}{\ln \frac{T_c - T_i}{T_c - T_o}} \tag{31}$$

The magma entering the heat exchanger has not flashed to equilibrium at the vaporizer pressure due to short-circuiting and the driving force for liquid-vapor heat-transfer in the boiling zone.

Hence

$$T_i = T_v + \Delta T_s \tag{32}$$

When ΔT_s is known, the LMTD can be evaluated using Eqs. (30) and (32).

The over-all heat-transfer coefficient, U, comprises the condensate and the magma film coefficients (h_c and h_{io} respectively) and the wall resistance ($1/h_w$).

$$\frac{1}{U} = \frac{1}{h_c} + \frac{1}{h_w} + \frac{1}{h_{io}} \tag{33}$$

Using conventional correlations for the film coefficients it can be shown that (see appendix I)

$$\frac{1}{U} = \frac{1}{K_c}\left(\frac{\phi_{mco}}{D_{to} N_t}\right)^{0.6} + \frac{D_{to} \ln \frac{D_{to}}{D_t}}{2\lambda_w} + \frac{1}{K_i} \frac{D_{to}}{(D_t v_t)^{0.8}} \tag{34}$$

where K_c and K_i contain the physical properties of the condensate and the suspension, respectively, λ_w is the thermal conductivity of the wall material and ϕ_{mco} is the condensate mass flow rate.

Combination of Eqs. (19), (20), (28) and (29) now yields

$$L_t = \frac{\phi_{mv}\, r}{U.\text{LMTD}} \cdot \frac{1+\beta}{\beta} \cdot \frac{2\sqrt{3}}{\pi^2} \cdot \left(\frac{\alpha D_t}{T}\right)^2 \cdot \frac{1}{D_{to}} \tag{35}$$

With the help of Eqs. (31) and (34) this equation will be used to calculate L_t as a function of α, β, D_t and v_t. The working volume of the system can thus be calculated when the brine height required to suppress boiling at the upper tubeplate is also known. For a given set of values of α, β, D_t and v_t; the heater pressure drop may be determined, which contributes significantly to the over-all resistance over the closed loop and, hence, to the specific power input. The heater geometry and the tube velocity accordingly play a dominant role in determining the second relationship between ϵ and V.

It should be noted that the tube length is limited by the following factors: 1) commercial availability, 2) mechanical considerations (e.g. tube vibrations) and 3) enhanced accumulation of condensate at the lower tube ends, reducing the condensate side film coefficient.

An extra allowance of 15% is taken into account in the evaluation of the actual heat-transfer surface area (i.e. L_t).

Circulation pressure drop and power consumed. The total circulation pressure drop, ΔP_c, can be described by the sum of the individual resistances based on heater tube velocity

$$\Delta P_c = \sum_{i=1}^{n} k_i \cdot \frac{1}{2} \rho_{SL} v_t^2 \qquad (N/m^2) \quad (36)$$

The pressure coefficients, k_i, are on the one hand constants, which may be taken from the literature (e.g. V.D.I. Wärme-Atlas) and on the other hand, for the tubes, functions of tube geometry and Fanning friction factor. An extra allowance of 25% will be included later in the calculation of the over-all pressure drop.

The effective power consumed by the axial-flow pump for mixing and circulation is given by

$$P_c = \frac{\phi_{vc} \Delta P_c}{\eta_p} \qquad (W) \quad (37)$$

where ϕ_{vc} is the volumetric rate of circulation and η_p is the over-all pumping efficiency. The specific power input then is

$$\epsilon = \frac{\phi_{vc} \Delta P_c}{\eta_p V \rho_{SL}} \qquad (W/kg) \quad (38)$$

The power consumption per ton capacity of salt, ϵ', is

$$\epsilon' = \frac{\phi_{vc} \Delta P_c}{\eta_p P} \qquad \left(W/\frac{kg}{s} \text{ or kWh/ton} \right) \quad (39)$$

Suspension of crystals. The minimum fluid velocity to attain suspension of the crystals may be taken from the literature on vertical hydraulic transport. According to Brauer (8) the minimum transport velocity is equal to five times the terminal velocity of the largest particles. For salt crystals of 1 mm size, the terminal velocity is for example approximately 0.1 m/s, resulting in a minimum upward velocity of 0.5 m/s. For the present crystallizer geometry the lowest system velocity is in the annular space below and above the heating element.

DESIGN INFORMATION FLOW DIAGRAM

The interrelationship between the design parameters and the equations derived previously is shown in the information flow diagram depicted in Figure 6. The diagram illustrates the sequence of calculation, starting from a set of

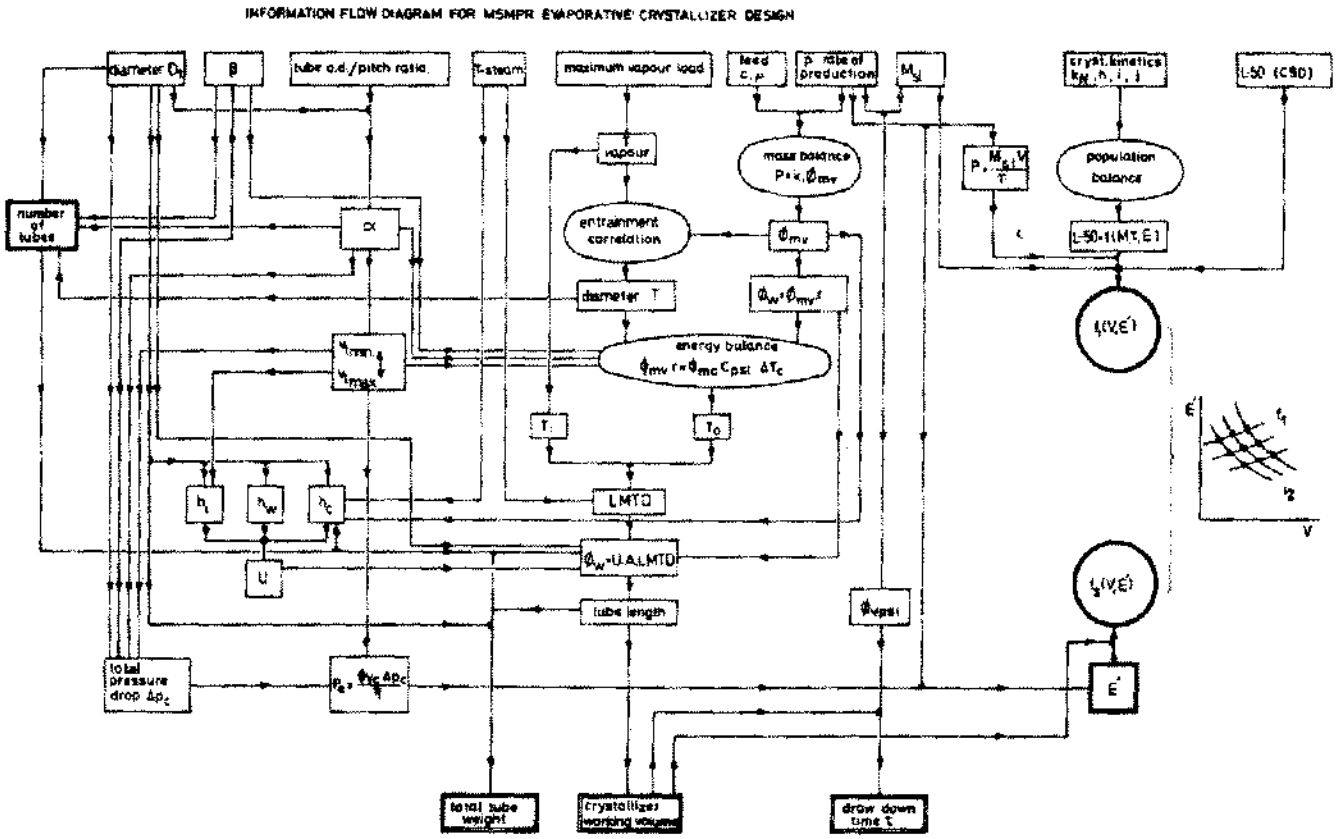

Figure 6. Interrelationship between design parameters and equations.

design input variables (the upper row of parameters in the diagram). The diagram comprises the following parts:

1) calculation of the power consumption per ton capacity of salt as a function of the crystallizer working volume, f_1 (V, ϵ'), on the basis of known kinetics of crystallization and given values of the rate of production, magma concentration and median crystal size and using the crystallization design relation; (Fig. 7)

2) evaluation of the rate of evaporation for given rate of production and feed composition using the mass balance equation. Next, calculation of the total heat load, ϕ_w, and the vaporizer diameter, T;

3) calculation of the heater tube length as a function of the tube velocity for a given set of values of D_t, β and α (or O.D./pitch ratio), using the energy balance over the heater and the equations for LMTD, U and L_t, respectively. The tube velocity is varied between the minimum slurry transport velocity in the tubes and a maximum velocity, which must be specified. The tube length determines the total tube weight of cupro-nickel and the crystallizer working volume. The total system pressure drop and the power consumption

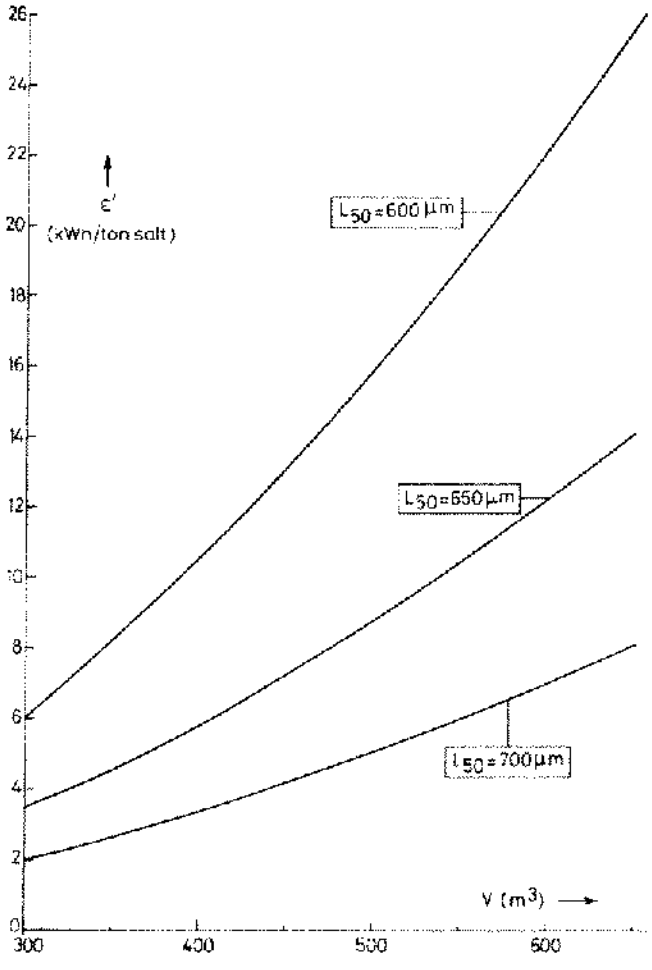

Figure 7. Plots of the crystallization relationship, f_1 (ϵ', Ω), for various median crystal size.

can be evaluated for the geometry and tube velocity chosen. The heat-transfer and pressure drop calculations thus result in a second set of data, f_2 (V, ϵ'), in numerical form, and

5) the solution to the design problem can finally be obtained from the points of intersection of arrays of curves representing f_1 (V, ϵ') and f_2 (V, ϵ') for various α, β and D_t. The design output data found for the point of intersection may be used for detail design so that equipment costs may be estimated in order to arrive at the optimum process configuration.

It should be noted that the present procedure does not include the design of the circulating pump. Also, restrictions on the concentration of those inorganic impurities, which may crystallize from the mother liquor, have not been imposed.

ILLUSTRATION OF THE DESIGN PROCEDURE

A number of computer programs have been used to perform the above calculations for variables α, β, D_t and v_t and to determine the points of intersection of the functions f_1 (V, ϵ') and f_2 (V, ϵ'). As stated, the calculations apply to the design of a crystallizer of the configuration shown in Figure 3. Table 2 lists the design input data which have been kept constant throughout the present calculations. Though the magma concentration can be freely chosen, a constant value of M_{SL} has been used here (Eq. (17) can be utilized to assess the effect of magma concentration, e.g. for constant specific power input, a lower value of M_{SL} will result in a larger crystallizer volume). The diameter of the vaporizer is 7 m and the steam demand is 27.4 kg/s for the operating conditions chosen (vapors supplied by a preceding effect are normally used for purposes of heating). It has been discussed previously that it is assumed that the crystallizer satisfies the MSMPR concept and that it is permitted to use the kinetic constants derived on the laboratory scale. The kinetic constants listed in Table 2 were obtained from preliminary experiments in the 50 liter MSMPR crystallizer and their applicability is actually limited to a smaller range of operating conditions compared with the constants reported in paragraph 3. The constants used are however sufficiently accurate for the present purpose.

Calculations in which the heater tube velocity was varied, have been performed for the combinations of parameters shown in Table 3. The function f_1 (V, ϵ') was evaluated for L_{50} = 400, 500, 600, 650 and 700 μm. Some of these curves are plotted in Figure 7. Typical results of heat-transfer and pressure drop calculations are shown in Table 4. Such data were used to construct plots representing f_2 (V, ϵ'). An example of a complete ϵ', V-diagram showing the crystallization curve for L_{50} = 650 μm and three heat-transfer/pressure drop curves for various α, is given in Figure 8. The points of intersection shown in this diagram represent three crystallizer operating points which all conform to identical design specifications. The points of intersection were

TABLE 2

Design Input Data

Rate of production	10 kg/s	($\sim 0.3 * 10^6$ t/a)
Magma concentration	365 kg/m^3	(ρ_{sl} = 1350 kg/m^3)
Feed concentration	320 kg/m^3	(saturated at 52°C)
Feed density	1185 kg/m^3	
Feed specific heat	3290 J/kg°C	
Vaporizer pressure	78 m bar	
Vapour temperature	47.5°C	
ΔT_S	2.5°C	
Heater inlet temperature	50 °C	
Steam condensation temperature	62 °C	(saturated steam)
Maximum vapour load	2.5 ton/m^2.h	
Minimum annular velocity	0.5 m/s	
Over-all pumping efficiency	50 %	
Density of salt crystals	2155 kg/m^3	
Specific heat of salt crystals	877 J/kg°C	
Specific heat of magma	2640 J/kg°C	
Dynamic viscosity of magma	$2.3 * 10^{-3}$ Ns/m^2	
Heat of vaporization	$2.38 * 10^6$ J/kg	
Boiling point elevation	6.5°C	
Height to suppress boiling at the upper tubeplate	2.4 m	
Kinetic constants	$k_N = 4 \times 10^{15}$, $n = 0.6$, $i = 1.5$, $j = 0.8$	

TABLE 3

Variation of Geometrical Design Parameters

tube diameter.			velocity ratio	tube diameter/pitch ratio
ASA (inch)	D_t (mm)	D_{to} (mm)	β	P/D_{to}
1.5	42.7	48.3	1	1.25 , 1.40 , 1.55
2.0	54.8	60.3	0.5 , 0.7 , 0.9 , 1.0 1.2 , 1.4 , 2.0 , 3.0	1.25 → 1.53 (8 steps)
3.0	82.8	88.9	0.5 , 1.0 , 3.0	1.25 , 1.40 , 1.55
4.0	108.2	114.3	1	1.25 , 1.40 , 1.55
6.0	161.5	168.3	1	1.25 , 1.40 , 1.55

TABLE 4

Typical Results of Heat-Transfer and Pressure Drop Calculations

	v_t (m/s)	V (m^3)	L_t (m)	A (m^2)	ΔP_c ($10^3 N/m^2$)	ϵ' (kWh/ton)	ΔT_c (C°)	total tube weight (ton)
$D_t = 54.7$mm	1.00	352	5.4	4155	3.35	1.71	2.0	94.8
$D_{to} = 60.3$mm	1.25	328	4.8	3674	4.60	2.93	1.6	83.8
$\alpha = 1.38$	1.50	312	4.3	3352	6.07	4.64	1.3	76.5
$\beta = 1$	1.75	300	4.0	3121	7.77	6.93	1.1	71.2
$N_t = 3908$	2.00	292	3.8	2946	9.68	9.86	1.0	67.2

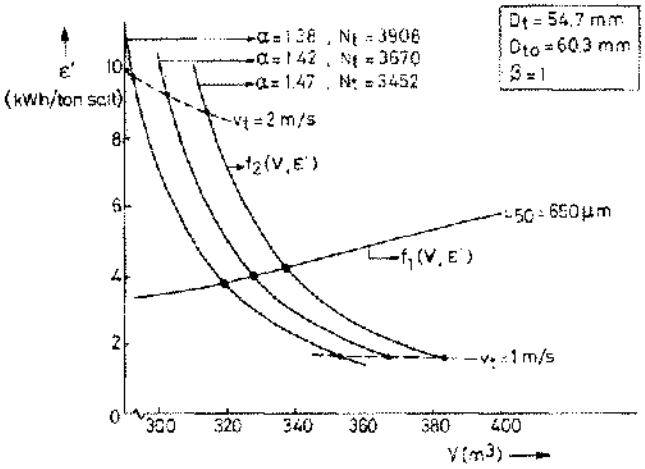

Figure 8. A ϵ'-V diagram for $L_{50} = 650$ μm and various α.

normally evaluated numerically. Crystallizer operating points are for instance listed in Table 5, illustrating the effect of α for $\beta = 1$, $D_t = 2''$ and $L_{50} = 650$ μm. The total tube weight is a rough measure for the equipment cost and may be directly used for preliminary cost-guestimation. The power consumption, ϵ', and the heating steam requirements contribute to the annual manufacturing cost (the total cost of electrical power is, however, usually much smaller than the steam cost).

The effects of tube diameter, velocity ratio β and pitch/tube diameter ratio α on crystallizer geometry and operating conditions in the operating point have been inferred from the above calculations. For the design situation given it was shown that at constant α and β large tube diameters are unfavorable both in terms of power consumption and crystallizer volume (tube length). For tubes smaller than 2" the resultant tube lengths were quite small, involving a large number of tubes to be installed. Attention was focused for these reasons on a configuration featuring 2" tubes.

The influence of the parameter α for 2" tubes and constant β was generally not very dramatic. Though increasing the pitch/diameter ratio results in an appreciable falling off in the number of tubes, the heat-transfer area and, hence, the total weight of cupro-nickel tubes are only slightly affected (compare Table 5). It was also demonstrated that the power consumption is not a strong function of α. The cost of the cupro-nickel tubes contributes significantly to the over-all equipment cost and the calculations thus indicate that the latter will not be very sensitive to variation of α.

Figure 9 depicts the general trends of the crystallizer volume, the power consumption, the number of tubes and the total weight as a function of β (all for the crystallizer operating point). The plots apply to 2" heater tubes, a median crystal size of 650 μm and two values of α. As opposed to α, the parameter β has a strong effect on the total tube weight and on the number of tubes, while the power consumption is more or less unaffected. A small value of β reduces the costs of cupro-nickel and the tubeplate manufacturing cost (less holes, smaller width which reduces tubeplate thickness) and should thus be chosen to minimize the overall equipment cost.

To complete the design procedure and optimize the design, the costs of the resulting crystallizers should be estimated as a function of α, D_t and especially β. Integral optimization would for instance involve assessment of tubeplate cost in dependence of the design parameters and would be rather cumbersome to accomplish. The costs of two alternatives with widely different values of β but conforming to the same design specifications, have been estimated to gain an impression of the comparative costs. The estimate is based on detail design of the crystallizer shown in Figure 3

TABLE 5

Crystallizer Operating Points as a Function of α for 2" Heater Tubes, $\beta = 1$ and $L_{so} = 650\ \mu m$

α	N_t	v_t (m/s)	V (m^3)	A (m^2)	ΔP_c ($10^3 N/m^2$)	ε' (kWh/ton)	ΔT_c (C°)	total tube weight (ton)
1.38	3908	1.39	317	3463	5.39	3.83	1.42	77.4
1.42	3670	1.45	326	3425	5.77	4.02	1.44	76.5
1.46	3452	1.50	336	3402	6.13	4.16	1.48	76.0
1.51	3254	1.57	345	3361	6.67	4.46	1.50	75.1
1.55	3072	1.63	356	3335	7.20	4.72	1.54	74.5
1.60	2905	1.69	366	3312	7.79	5.00	1.57	74.0
1.64	2751	1.74	378	3300	8.36	5.24	1.61	73.7
1.68	2609	1.80	389	3281	9.06	5.57	1.64	73.3

fitted with expansion bellows in the outer shell of the heating element. The design characteristics and associated costs are listed in Table 6. It may be seen from these data that the tubeplate cost differs by a factor of 2 and the over-all equipment cost by a factor of 1.3, for $\beta = 0.5$ and $\beta = 3$, respectively. These differences seem to be sufficiently substantial to justify the adoption of the proposed design method in actual practice.

SUMMARY AND CONCLUSIONS

The characteristics of salt crystallizers with internal and external circulation have been discussed and a summary has been given of the results of experiments carried out in a pilot-scale and a bench-scale crystallizer. The problem of equipment selection has been dealt with on the basis of the comparative merits of both types of salt crystallizer. An integral design procedure for crystallizers with internal circulation has been put forward. In the development of the design algorithm it has been attempted to integrate thermal and hydraulic design with requirements of crystal size distribution. Calculations have been performed to illustrate the design method and to investigate the effect of the geometry of draft tube and heating element on the resultant process configuration. The ratio of draft tube velocity and velocity in the annulus was shown to be an important design factor, strongly affecting the total heater tube weight. Over-all equipment costs of two crystallizers with different velocity ratio (but conforming to the same design specifications) were found to differ by 30% or Dfl 10^6. The results of the calculations suggest that it may be worth-while to devote adequate attention to salt crystallizer design and that the proposed design procedure may essentially be applied industrially.

APPENDIX I

Evaluation of overall heat-transfer coefficient.

$$\frac{1}{U} = \frac{1}{h_c} + \frac{1}{h_w} + \frac{1}{h_{so}} \qquad \text{(Eq. 33)}$$

Outside film coefficient:

$$h_c = 1.8(Re_c)^{-1/3}\left(\frac{\lambda_c^3 \rho_c^2 g}{\eta_c^2}\right)^{1/3} \qquad (I.1)$$

where

$$Re_c = \frac{4\,\phi_{mco}}{\pi \eta_c D_{to} N_t} \qquad (I.2)$$

and: λ_c, ρ_c and η_c are the thermal conductivity, density and dynamic viscosity of the condensate, respectively, ϕ_{mco} is the condensate mass flow rate, which is approximately equal to the rate of evaporation. Eq. (I.1) may be written

$$h_c = K_c\left(\frac{D_{to} N_t}{\phi_{mco}}\right)^{1/3} \qquad (W/m^2.C) \qquad (I.3)$$

where

$$K_c = \left(\frac{\pi \lambda_c^3 \rho_c^2 g}{4 \eta_c}\right)^{1/3} \qquad (I.4)$$

Wall resistance:

$$h_w = \frac{2 \lambda_w}{D_{to} \ln \frac{D_{to}}{D_{ti}}} \qquad (W/m^2.C) \qquad (I.5)$$

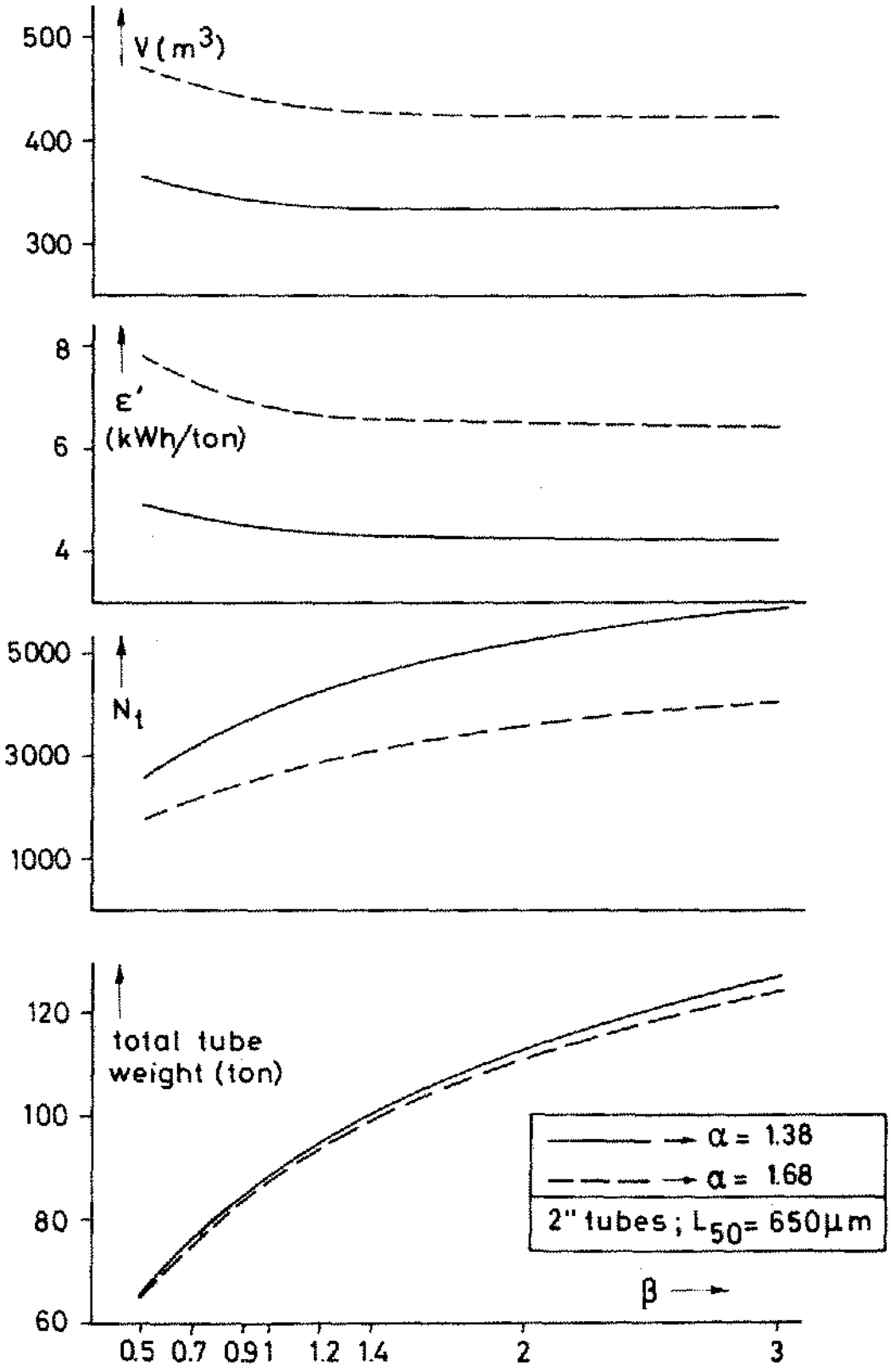

Figure 9. Crystallizer volume, power consumption, number of heater tubes and total tube weight as a function of β.

TABLE 6

Detail Design and Costs of Two Alternatives for P = 10 kg/s, M_{sL} = 365 kg/m³, L_{50} = 650 μm

	VESSEL I	VESSEL II
β	0.5	3.0
tube diameter	2"	2"
α	1.51	1.51
T (m)	7	7
D_d (m)	5.7	4.0
tubeplate width (m)	0.64	1.5
N_t	2170	4340
total tube weight (ton)	64.6	111.7
heat-transfer area (m^2)	2892	5000
L_t (m)	6.75	5.80
V (m^3)	404	368
v_t (m/s)	1.8	1.5
over-all height of vessel (m)	21.4	20.4
total vessel weight (ton)	250	300
vessel wall thickness (mm)	20-26	20 - 26
thickness tubeplate (mm) (monel clad mild steel)	75+10	90 + 10
tubeplate cost (10^3 Dfl) (incl. manufacturing cost)	310	635
over-all equipment cost (10^6Dfl) (excl. axial-flow pump)	3.39	4.34

where λ_w is the thermal conductivity of the wall material. h_w is based on the outer heat-transfer area.

Inside film coefficient:

$$Nu = 0.027\ Re^{0.8}\ Pr^{1/3} \tag{I.6}$$

or

$$\frac{h_i D_t}{\lambda_L} = 0.027\left(\frac{D_t v_t \rho_{sL}}{\eta_{sL}}\right)^{0.8}\left(\frac{c_{psL}\,\eta_{sL}}{\lambda_L}\right)^{1/3} \tag{I.7}$$

where η_{sL} is the dynamic viscosity of the slurry and λ_L is the thermal conductivity of the mother liquor.

Rearranging gives

$$h_i = K_i \frac{v_t^{0.8}}{D_t^{0.2}} \tag{I.8}$$

where

$$K_i = 0.027\,\frac{\lambda_L^{2/3}\rho_{sL}^{0.8}\,c_{psL}^{1/3}}{\eta_{sL}^{0.47}} \tag{I.9}$$

h_i must be based on the outer heat-transfer area. Hence

$$h_{io} = \frac{D_t}{D_{to}} h_i = K_i \frac{(D_t\ v_t)^{0.8}}{D_{to}} \tag{I.10}$$

By combination of Eqs. (I.3), (I.5) and (I.10) the overall heat-transfer coefficient can be written

$$\frac{1}{U} = \frac{1}{K_c}\left(\frac{\phi_{mco}}{D_{to} N_t}\right)^{1/3} + \frac{D_{to}\ln\frac{D_{to}}{D_t}}{2\,\lambda_w} + \frac{1}{K_i}\frac{D_{to}}{(D_t v_t)^{0.8}} \tag{I.11}$$

Notation.

A	heat transfer surface area	m^2
B°	rate of nucleation	$\#/m^3.s$
c_f	salt concentration in feed	kg/m^3
c_p	salt concentration in product stream	kg/m^3
c_{pf}	specific heat of feed	J/kg°C
c_{pSL}	specific heat of magma	J/kg°C
D_d	draft tube diameter	m
D_i	impeller diameter	m
D_t	inner heater tube diameter	m
D_{to}	outer heater tube diameter	m
G	linear crystal growth rate	m/s
g	gravitational constant	m/s^2
H_b	brine level in vaporizer	m
h_c	condensate heat-transfer coefficient	$W/m^2.°C$
h_i	inside (magma) heat-transfer coefficient	$W/m^2.°C$
h_{io}	h_i based on tube O.D.	$W/m^2.°C$
h_w	wall heat-transfer coefficient	$W/m^2.°C$
h, i, j	kinetic constants	—
k_n	nucleation rate coefficient	—
k_v	volume shape factor of crystals	—
k_c	constant in crystallization design relation	—
K_c	constant in equation for h_c	—
K_i	constant in equation for h_i	—
k_l	pressure drop coefficient	—
L	crystal size	m, μm
L_{50}	median crystal size	m, μm
L_t	heater tube length	m
LMTD	logarithmic mean temperature difference	°C
M_{SL}	magma concentration	kg/m^3
n	population density	$/m^4$
N_t	total number of heater tubes	—
p	heater tube pitch	m
P	rate of salt production	kg/s
P_e	power consumption of circulating pump	W
ΔP_c	closed loop pressure drop	N/m^2
Q_{cr}	heat of crystallization	J/kg
r	heat of vaporization	J/kg
Re_c	Reynolds number for condensate film	—
T	vaporizer diameter	m
T_f	feed temperature	°C
T_p	product temperature	°C
T_v	vapor temperature	°C
T_i	heater inlet temperature	°C
T_o	heater outlet temperature	°C
T_c	condensation temperature	°C
ΔT_c	temperature rise through the heater	°C
ΔT_s	difference between T_i and T_v	°C
U	over-all heat-transfer coefficient	$W/m^2.°C$
V	crystallizer suspension volume	m^3
v_a	velocity in the annulus	m/s
v_t	heater tube velocity	m/s
v_d	draft tube velocity	m/s
α	pitch/tube diameter ratio	—
β	annular to draft tube velocity ratio	—
ϵ	specific impeller power input	W/kg
ϵ'	power consumption per ton capacity of salt	kWh/ton
λ_c	thermal conductivity of condensate	W/m.°C
λ_w	thermal conductivity of wall	W/m.°C
λ_l	thermal conductivity of mother liquor	W/m.°C
η_c	viscosity of condensate	Ns/m^2
η_p	over-all pumping efficiency	—
ρ	density	kg/m^3
ϕ_v	volumetric flow rate	m^3/s
ϕ_m	mass flow rate	kg/s
ϕ_w	heat flow rate	W
τ	draw-down time	s

ACKNOWLEDGEMENT

The authors wish to thank the Nederlandsche Electrolasch Maatschappij, Leiden, The Netherlands, for performing the detail salt crystallizer design and the cost estimations and for the helpful suggestions.

REFERENCES

1. Asselbergs, C.J. and de Jong, E.J. 1976. Integral design of crystallizers as illustrated by the design of a continuous stirred-tank cooling crystallizer, In Industrial Crystallization, J.W. Mullin (ed.). New York, Plenum Press.
2. Rutten, J.J. and de Jong, E.J. 1969. Factors affecting the rate of evaporation in a cylindrical evaporator body with tangential inlet. Paper presented at the 3rd CHISA Congress, Symp. Ind. Crystallization, Czechoslovakia.
3. Land, C.M. van 't and de Waal, K.J.A. 1973. Aspects of technical crystallization of sodium chloride. Research within AKZO (1973), 90–94.
4. Land, C.M. van 't and Wienk, B.G. 1976. Control of particle size in industrial NaCl-crystallization. In Industrial Crystallization, J.W. Mullin (ed.). New York, Plenum.
5. Asselbergs, C.J. 1978. A study of factors in operation and design of evaporating crystallizers for salt. Delft, University of Technology, Doctoral Thesis (The Netherlands).
6. Larson, M.A. and Randolph, A.D. 1971. Theory of particulate processes. New York, Academic Press.
7. Ottens, E.P.K. 1973. Nucleation in continuous agitated crystallizers. Delft, University of Technology, 1973 (The Netherlands).
8. Brauer, H. 1971. Grundlagen der Einphasen- und Mehrphasenströmung. Aarau, Verlag Sauerländer.